Engineering Structures 292 (2023) 116515

Contents lists available at ScienceDirect

Engineering Structures

journal homepage: www.elsevier.com/locate/engstruct

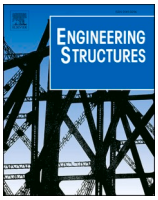

Mobile crowdsensing framework for drive-by-based dense spatial-resolution bridge mode shape identification

Zhen Peng [a], Jun Li [a,*], Hong Hao [a,b], Ning Yang [c]

[a] Centre for Infrastructural Monitoring and Protection, School of Civil and Mechanical Engineering, Curtin University, WA 6102, Australia
[b] Earthquake Engineering Research and Test Center, Guangzhou University, Guangzhou, China
[c] School of Civil Engineering, Fujian University of Technology, Fuzhou, China

ARTICLE INFO

Keywords:
Drive-by
Mobile crowdsensing
Sparse matrix completion
Mode shape identification
Structural Health Monitoring

ABSTRACT

Moving vehicles equipped with various types of sensors can efficiently monitor the health conditions of a population of transportation infrastructure such as bridges. This paper presents a mobile crowdsensing framework to identify dense spatial-resolution bridge mode shapes using sparse drive-by measurements. The proposed method converts mode shape identification into a physical-informed optimization problem with two objective function terms. The first objective minimises the mode shape identification error based on the fact that the ratio of a specific order mode shape value at any two locations is time-invariant. Since the bridge mode shape should be globally smooth even when the local stiffness is discontinuous, the smoothness of the identified mode shape is introduced as the second objective. The feasibility and advantages of the proposed model are verified numerically and through large-scale experimental studies. Numerical results demonstrate that the proposed method can efficiently identify bridge mode shapes with a desirable accuracy. The adverse effects of road roughness and measurement noise on the mode shape identification accuracy are substantially suppressed by introducing crowdsensing and making use of collected responses over multiple trips. The applicability of the proposed method for bridges having varying cross sections and multiple spans is also studied. A series of drive-by tests with different vehicle masses and speeds are conducted on a large-scale footbridge. The experimental results verify that the proposed method can accurately identify the bridge mode shapes and is robust to vehicle mass and speed variation. The identification accuracy of large-scale bridge mode shapes using crowdsensing drive-by measurements is demonstrated in this study.

1. Introduction

Bridge structures play a critical role in transportation infrastructure by carrying highway traffic loads, crossing natural obstacles, and enabling effective communication between two destinations. As of 2020, there were more than 617,000 and 912,000 bridges across the United States and China, respectively [1]. According to the 2021 Bridge Conditions Report of the American Road & Transportation Builders Association, more than 45,000 bridges were in poor condition and classified as "structurally deficient" in 2020 [2]. With an increasing number of bridges approaching the end of their designed lifespan, developing guidelines and securing funding for bridge safety evaluation and maintenance are crucial to ensure the serviceability and safety of existing bridges [3]. Bridge structural health monitoring (BSHM) systems generally comprise the design, development, and implementation of damage detection or characterisation strategy for the real-time assessment of structural conditions [4]. Over the past decades, BSHM has been widely recognised as an effective technique for revealing the structural performance degradation and evaluating the health condition of bridges under operational conditions [5].

However, recording structural vibration data using traditional BSHM systems with fixed sensor networks is costly and time consuming owing to labour expenses and installation demands, especially when monitoring large-scale bridges using wired sensor networks that require complex installations of long cables [6]. Numerous fixed sensors need to be installed on each monitored bridge to obtain sufficient spatial dense-mode shapes [7]. Given a high number of assets and a limited budget, it is currently unfeasible to scale up on-site structural health monitoring

* Corresponding author at: Centre for Infrastructural Monitoring and Protection, School of Civil and Mechanical Engineering, Curtin University, WA 6102, Australia.
E-mail address: junli@curtin.edu.au (J. Li).

https://doi.org/10.1016/j.engstruct.2023.116515
Received 10 December 2022; Received in revised form 18 May 2023; Accepted 19 June 2023
Available online 27 June 2023

(SHM) systems for every bridge. To provide alternatives to and overcome constraints of traditional SHM systems, new techniques are being explored to develop low-cost, scalable, and easily deployable systems. Drones [8], vision-based monitoring [9], crowdsensing [10] and earth observation satellites [11] are some examples of emerging techniques.

The drive-by approach has gained popularity because of its low cost, high efficiency, and potential for scalable bridge condition assessment [12]. Yang et al. [13] theoretically verified the feasibility of extracting the first several bridge frequencies from the vehicle responses, and investigated the effects of vehicle speed, bridge/vehicle frequency ratios and bridge/vehicle mass ratios on the vehicle-bridge interaction responses [14]. The results indicate that higher vehicle speeds can lead to greater amplitudes of the bridge frequency. This can be advantageous for extracting the bridge frequency from vehicle responses. Subsequently, numerical [15], experimental [16] and in-situ studies [17] have been conducted to investigate the factors that may affect the accuracy of drive-by bridge modal identification. The success of drive-by bridge modal identification largely depends on the precondition that the bridge's dynamic behaviour is well-excited by vehicle loads and other environmental factors.

Drive-by SHM methods that leverage sensors on passing vehicles to indirectly identify the bridge frequency, mode shape, and structural damage have been well studied and validated [18]. Owing to the high mobility of vehicles, it is possible to identify the dense spatial-resolution mode shape from drive-by monitoring methods, which is advantageous for bridge damage localisation [19]. Drive-by SHM can incorporate the mobile crowdsensing technique to monitor the health condition of a population of bridges with low costs [20]. According to the Golden Gate Bridge Highway and Transportation District, the average daily traffic volume of this bridge is approximately 112,000–119,000. The bridge modal information can be continuously monitored and updated timely, even if only one percent of the passing vehicles share the decentralized GPS and acceleration data to the crowdsensing database. This has sparked a great interest in crowdsensing for drive-by SHM. Yang et al. [13] theoretically demonstrated the feasibility of extracting the bridge frequencies and mode shapes from vehicle-bridge coupled vibration responses. Methods using cross-spectrum estimation [17], contact point response identification [21] and novel time–frequency analysis [22] have been recently proposed to improve the identifiability and accuracy of drive-by- bridge natural frequency and mode shape identification. More recently, the dynamic interaction between a passing vehicle and a simply supported beam with local structural damage was derived in Ref. [23]. It was found that the dynamic responses of a passing vehicle contain structural damage information.

The majority of existing drive-by modal identification and damage detection researches focus on analytical and numerical studies and experimental tests of scaled models [24]. At present, only a few of studies have been reported to identify the natural frequencies and mode shapes from the full-scale structures using drive-by methods. The following challenges that prevent the full-scale structure applications can be identified from previous studies: (i) the amplitude of vehicular vibrations may be an order of magnitude larger than that of the bridge, which makes it difficult to separate the desired bridge vibration from the drive-by measurements [25]; (ii) the vehicle–bridge contact point displacement is a linear combination of road roughness and bridge responses. Thus, the modal identification accuracy can be adversely affected by the pavement profile [26]; (iii) the external excitation and bridge damping coefficient affect the mode shape identification based on the instantaneous amplitude envelopes of the vehicle vibrations [27]; (iv) under typical vehicle speeds, the interaction time between the vehicle and the bridge may be too short to obtain the mode shapes by using the existing short-time frequency domain decomposition (FDD) [28] and stochastic subspace identification methods [29].

Fig. 1(a) and (b) show schematic demonstration of the sparse matrices generated by fixed and moving sensor networks, respectively. The data stream produced by the traditional SHM system with a fixed sensor network is temporally dense but spatially sparse. In comparison, the structural responses recorded by moving vehicles are a sparse scan of the bridge full-field dynamic response matrix with temporal and spatial dimensions. In the case of a vehicle passing the bridge at a constant speed, the vehicle–bridge contact point scans the diagonal element of the full-field matrix. The unobserved part of the full-field response

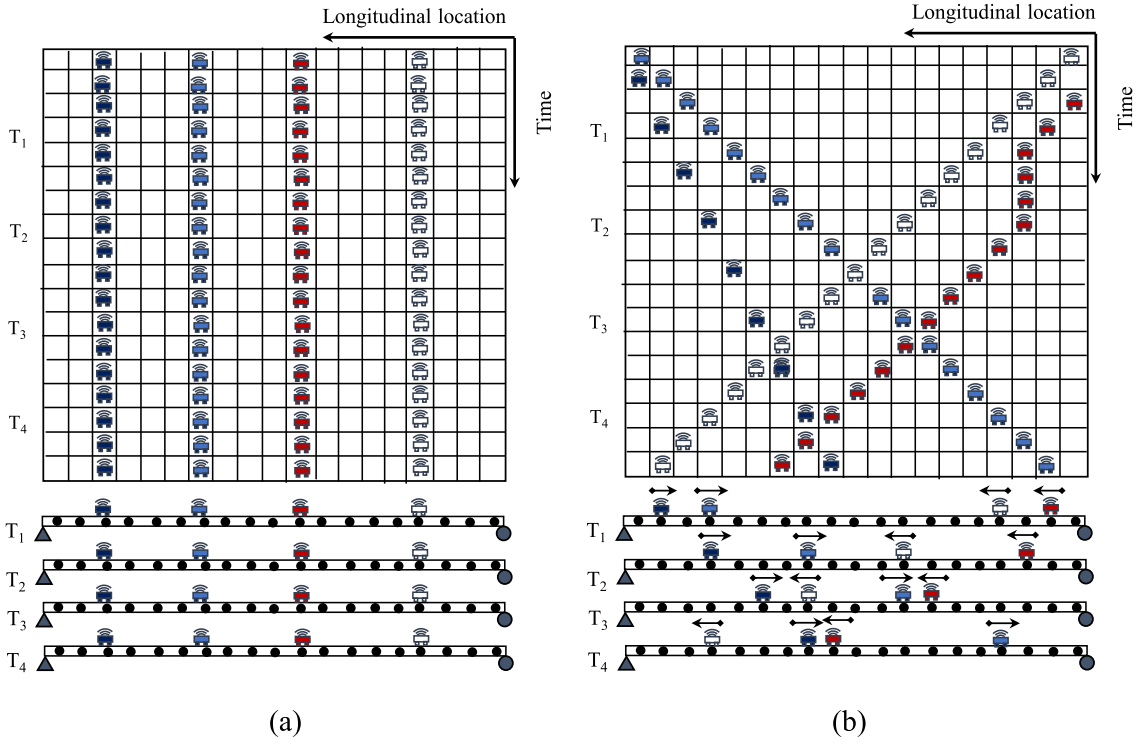

Fig. 1. Schematic demonstrations of sparse matrices generated by: (a) SHM system with fixed sensor network: and (b) moving sensor network.

matrix can be reconstructed from the available moving sensing entries using the modern matrix completion technique [30,31]. Sparse matrix completion is a popular research topic in machine learning and is widely used in recommendation systems. Recently, it has been successfully applied to bridge system identification using moving sensors. Once the full-field response matrix is reconstructed, the modal properties such as mode shapes and damping ratios, can be identified using modal order reduction techniques, such as principal component analysis, singular value decomposition, and proper orthogonal decomposition. In Ref. [31], the feasibility of using the matrix completion method to extract bridge frequencies, damping and mode shapes from data collected by a large vehicular sensor network was numerically investigated. The modal identification error was under 2% when more than 50 moving vehicles synchronously scanned the bridge responses. However, the efficiency of deploying such a population of vehicles moving on the bridge and the synchronisation of data from moving sensor networks should be further investigated. The goal of matrix completion is to simultaneously obtain both the optimal low-rank mode shape and the generalised modal coordinate. Intuitively, it is challenging to discover both of them from a super-sparse response matrix produced by fewer vehicle scans. Therefore, additional physical insights and constraints need to be imposed to increase matrix completion accuracy using fewer vehicles. In fact, the low-rank mode shapes are related to the structural stiffness and mass matrix, which can serve as a damage feature. The generalised modal coordinate is related to the structural damping property and external excitation. In contrast, the generalised modal coordinate can be calculated once the mode shape is obtained. Taking these considerations into account, this study attempts to preferentially identify the mode shapes from the sparse responses scanned by moving vehicles. The proposed method is based on the fact that the ratio of a specific order mode shape value at any two particular locations is constant at any time.

This paper proposes a mobile crowdsensing framework to identify dense spatial-resolution bridge mode shapes using sparse drive-by measurements. The mode shape identification problem is converted to a physical-informed optimization problem with two objective function terms to overcome the matrix completion accuracy associated with fewer vehicles. The mobile crowdsensing technique and a strategy of incorporating multiple vehicle trips data are introduced to suppress the adverse effects of road roughness, vehicle speed and measurement noise. Numerical and experimental studies are conducted to verify the feasibility and superiority of the proposed approach.

2. Methodology

The equation of motion of the beam bridge structure is given as

$$EI\frac{\partial^4 y(x,t)}{\partial x^4}+\overline{m}\frac{\partial^2 y(x,t)}{\partial t^2}+\mu\frac{\partial y(x,t)}{\partial t}=F(x,t) \tag{1}$$

where $\overline{m}$, μ, and EI represent the mass of material per unit length, damping parameter and flexural rigidity of the bridge, respectively; $F(x,t)$ denotes the external excitation applied at the location $\times$ from the left end of the bridge and the time instant t; The full-field displacement response $y(x,t)$ at location x and time instant t can be approximated as the superposition of the mode-shape vectors

$$y(x,t)\approx\sum_{i=1}^{r}\xi_i(t)\phi_i(x) \tag{2}$$

where $\phi_i(x)$ is the i-th mode shape value at the location x, and $\xi_i(t)$ is the generalised coordinate for the i-th mode at the time instant t, r denotes the modal truncation order.

As illustrated in Fig. 2, only a sparse subset of $\boldsymbol{y}$ is obtained as $\boldsymbol{y}_{obs}$ by using the sensors on moving vehicles. The sparse observable $\boldsymbol{y}_{obs}$ is expressed as follows

$$\boldsymbol{y}_{obs}=\mathbf{S}(\boldsymbol{y}) \tag{3}$$

where $\mathbf{S}$ denotes the sparse entries selection matrix, which can be obtained from the real-time vehicle location when it passes the bridge.

When a vehicle crosses the bridge, the suspension system acts as a low-pass filter for bridge vibration and road roughness. Vehicle–bridge contact point responses are widely recognised to outperform vehicle body responses in extracting bridge modal properties [21]. The vehicle–bridge contact point displacement is a linear combination of road roughness and bridge responses, which do not contain the vehicle vibration component. Therefore, the contact point forces are identified from the vehicle body responses using a general Kalman filter with unknown inputs (GKF-UI). The contact point displacement can be calculated from the contact point force divide by the vehicle tire stiffness. After contact force identification, the drive-by bridge mode shape identification is conducted to extract the bridge mode shape. Previous studies have used additional signal processing procedures to further separate the bridge vibration responses from road roughness and measurement noise [32,33]. These methods usually eliminate the adverse effects of road roughness by subtracting the responses measured from the front and real axes or two adjacent trips [34]. They are based on the basic assumption that the road roughness scanned by the two vehicle travelling trips is the same. This assumption is satisfied when the

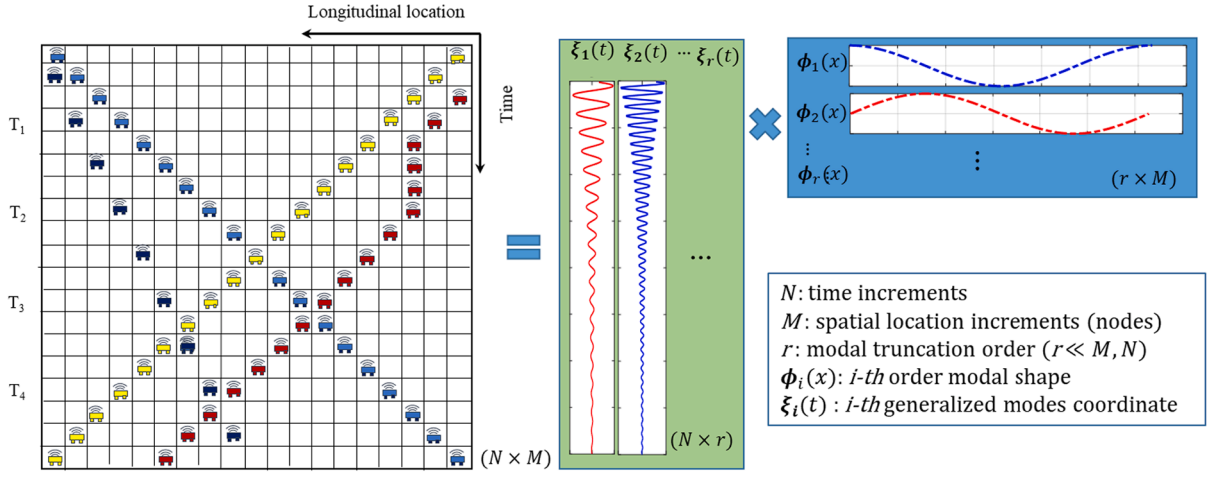

Fig. 2. Concept of modal decomposition from sparse responses measured from moving vehicle.

running trajectories of these two vehicle travelling trips as well as the tire characteristics coincide perfectly, which may not be sufficiently practical. To extend the feasibility of the proposed approach to more general situations, the crowdsensing concept is introduced in this study to integrate vibration responses of multiple trips, for eliminating the effect of road roughness and measurement noise-induced uncertainties on bridge modal identification using drive-by techniques.

2.1. GKF-UI based vehicle–bridge contact point response identification

The contact point displacement is a linear combination of road roughness and bridge responses, which can be considered as the external base-excited input applied to the vehicle system in the vertical direction. The representative frequency response function (FRF), Kalman filter, and deconvolution-based force identification methods can be used to extract the contact point responses from the vehicle responses. In this study, the GKF-UI method proposed by Huang et al. [35] to identify the unknown external input without direct feedback at unknown excitation, is adopted. For the commonly used 2- degree of freedom (DOF) quarter-car model as shown in Fig. 3, the contact point displacement induced input f_{s1} is of interest and can be identified by using the measured vehicle body acceleration response $\ddot{x}_{b1}$. The theoretical derivation of the GKF-UI is briefly introduced in the remainder of this section.

Defining $\boldsymbol{x} = [x_{s1}, x_{b1}]^T$, the quarter-car model equation of motion can be written as

$$\boldsymbol{m}_v\ddot{\boldsymbol{x}}_v + \boldsymbol{c}_v\dot{\boldsymbol{x}}_v + \boldsymbol{k}_v\boldsymbol{x}_v = \boldsymbol{f}^u \tag{4}$$

where $\boldsymbol{m}_v = \begin{bmatrix} m_{s1} & 0 \\ 0 & m_{b1} \end{bmatrix}$, $\boldsymbol{c}_v = \begin{bmatrix} c_{b1}+c_{s1} & -c_{b1} \\ -c_{b1} & c_{b1} \end{bmatrix}$, $\boldsymbol{k}_v = \begin{bmatrix} k_{b1}+k_{s1} & -k_{b1} \\ -k_{b1} & k_{b1} \end{bmatrix}$, $\boldsymbol{f}^u = \begin{bmatrix} f_{s1} \\ 0 \end{bmatrix}$, and $\boldsymbol{x}_v = \begin{bmatrix} x_{s1} \\ x_{b1} \end{bmatrix}$.

Eq. (4) can be rewritten into the system state equation as

$$\dot{\boldsymbol{Z}} = \begin{bmatrix} \dot{\boldsymbol{x}}_v \\ \ddot{\boldsymbol{x}}_v \end{bmatrix} = \begin{bmatrix} 0 & \boldsymbol{I} \\ -\boldsymbol{m}_v^{-1}\boldsymbol{k}_v & -\boldsymbol{m}_v^{-1}\boldsymbol{c}_v \end{bmatrix}\begin{bmatrix} \boldsymbol{x}_v \\ \dot{\boldsymbol{x}}_v \end{bmatrix} + \begin{bmatrix} 0 \\ \boldsymbol{m}_v^{-1} \end{bmatrix}\begin{bmatrix} f_{s1} \\ 0 \end{bmatrix} = \boldsymbol{A}\boldsymbol{Z} + \boldsymbol{B}\boldsymbol{f}^u \tag{5}$$

where $\boldsymbol{A}$ is the state transformation matrix, and $\boldsymbol{B}$ is the influence matrix of the external input. Eq. (5) is discretised into the following equation

$$\boldsymbol{Z}_{k+1} = \boldsymbol{A}_k\boldsymbol{Z}_k + \boldsymbol{B}_k\boldsymbol{f}_k^u + \boldsymbol{B}_{k+1}\boldsymbol{f}_{k+1}^u + \boldsymbol{w}_k \tag{6}$$

in which $\boldsymbol{A}_k = e^{\boldsymbol{A}\Delta t}$; $\boldsymbol{B}_k = \left[\boldsymbol{A}_k - (\boldsymbol{A}_k - \boldsymbol{I})(\boldsymbol{A}\Delta t)^{-1}\right](\boldsymbol{A}\Delta t)^{-1}(\boldsymbol{B}\Delta t)$; $\boldsymbol{B}_{k+1} = \left[(\boldsymbol{A}_k - \boldsymbol{I})(\boldsymbol{A}\Delta t)^{-1} - \boldsymbol{I}\right](\boldsymbol{A}\Delta t)^{-1}(\boldsymbol{B}\Delta t)$, where Δt denotes the sampling interval, $\boldsymbol{I}$ is the unit matrix , $\boldsymbol{w}_k$ represents the process noise (or model uncertainty) with zero mean, and the covariance matrix $E[\boldsymbol{w}\boldsymbol{w}^T] = \boldsymbol{Q}$. It is noted that $\boldsymbol{Q}$ is the covariance matrix of process noise.

Given the measured vehicle body acceleration response $\ddot{x}_{b1}$, the measurement equation can be written as

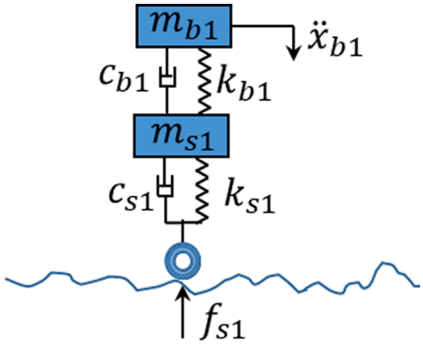

Fig. 3. The used quarter-car model.

$$\begin{aligned} \boldsymbol{y}_{k+1} = \ddot{x}_{b1,k+1} &= \left[m_{b1}^{-1}k_{b1} - m_{b1}^{-1}k_{b1}m_{b1}^{-1}c_{b1} - m_{b1}^{-1}c_{b1}\right]\begin{bmatrix} x_{s1,k1} \\ x_{b1,k1} \\ \dot{x}_{s1,k1} \\ \dot{x}_{b1,k1} \end{bmatrix} \\ &= \boldsymbol{C}_{k+1}\boldsymbol{Z}_{k+1} + \boldsymbol{V}_{k+1}, \end{aligned} \tag{7}$$

where $\boldsymbol{y}_{k+1}$ represents the observation at the time instant $t = (k+1)\Delta t$, $\boldsymbol{C}_{k+1}$ is the measurement matrix, $\boldsymbol{V}_{k+1}$ is the measurement noise that is assumed as the Gaussian white noise process with zero mean value and covariance matrix of $E\left[\boldsymbol{V}_{k+1}\boldsymbol{V}_{k+1}^T\right] = \boldsymbol{R}_{k+1}$, and $\boldsymbol{R}_{k+1}$ is the covariance matrix of measurement noise at discrete time instant $t = (k+1)\Delta t$, in which Δt is the sampling time step.

The GKF-UI has two main steps. First, the time prediction of the structural state $\widetilde{\boldsymbol{Z}}_{k+1|k}$ is conducted as follows

$$\widetilde{\boldsymbol{Z}}_{k+1|k} = \boldsymbol{A}_k\widehat{\boldsymbol{Z}}_{k|k} + \boldsymbol{B}_k\widehat{\boldsymbol{f}}_{k|k}^u + \boldsymbol{B}_{k+1}\widehat{\boldsymbol{f}}_{k+1|k+1}^u \tag{8}$$

Then, the estimated $\widehat{\boldsymbol{Z}}_{k+1|k+1}$ in the measurement updating procedure is derived as

$$\widehat{\boldsymbol{Z}}_{k+1|k+1} = \widetilde{\boldsymbol{Z}}_{k+1|k} + \boldsymbol{K}_{k+1}\left(\boldsymbol{y}_{k+1} - \boldsymbol{C}_{k+1}\widetilde{\boldsymbol{Z}}_{k+1|k}\right) \tag{9}$$

$$\boldsymbol{K}_{k+1} = \widetilde{\boldsymbol{P}}_{k+1|k}^{\boldsymbol{Z}}\boldsymbol{C}_{k+1}^T\left(\boldsymbol{C}_{k+1}\widetilde{\boldsymbol{P}}_{k+1|k}^{\boldsymbol{Z}}\boldsymbol{C}_{k+1}^T + \boldsymbol{R}_{k+1}\right)^{-1} \tag{10}$$

where $\widetilde{\boldsymbol{P}}_{k+1|k}^{\boldsymbol{Z}}$ is the error covariance matrix at the prediction stage. Here, Δ_{k+1} is defined as

$$\begin{aligned} \Delta_{k+1} &= \mathbf{y}_{k+1} - \widehat{\mathbf{y}}_{k+1|k+1} \\ &= (\mathbf{I} - \mathbf{C}_{k+1}\mathbf{K}_{k+1})\left(\mathbf{y}_{k+1} - \mathbf{C}_{k+1}\left(\mathbf{A}_k\widehat{\mathbf{Z}}_{k|k} + \mathbf{B}_k\widehat{\mathbf{f}}_{k|k}^u\right) - \mathbf{C}_{k+1}\mathbf{B}_{k+1}\widehat{\mathbf{f}}_{k+1|k+1}^u\right) \end{aligned} \tag{11}$$

By minimizing Δ_{k+1}, $\widehat{\mathbf{f}}_{k+1|k+1}^u$ is obtained by using least-squares estimation as

$$\widehat{\mathbf{f}}_{k+1|k+1}^u = \mathbf{S}_{k+1}\left(\mathbf{y}_{k+1} - \mathbf{C}_{k+1}\left(\mathbf{A}_k\widehat{\mathbf{Z}}_{k|k} + \mathbf{B}_k\widehat{\mathbf{f}}_{k|k}^u\right)\right) \tag{12}$$

where

$$\begin{aligned} \mathbf{S}_{k+1} = &\left[(\mathbf{C}_{k+1}\mathbf{B}_{k+1})^T\left(\mathbf{C}_{k+1}\widetilde{\mathbf{P}}_{k+1|k}^{\mathbf{z}}\mathbf{C}_{k+1}^T + \mathbf{R}_{k+1}\right)^{-1}(\mathbf{C}_{k+1}\mathbf{B}_{k+1})\right]^{-1} \\ &(\mathbf{C}_{k+1}\mathbf{B}_{k+1})^T\left(\mathbf{C}_{k+1}\widetilde{\mathbf{P}}_{k+1|k}^{\mathbf{z}}\mathbf{C}_{k+1}^T + \mathbf{R}_{k+1}\right)^{-1} \end{aligned} \tag{13}$$

The other error covariance matrices used in the procedure can be found in Ref. [35]. Thus, following the procedures of the GKF-UI algorithm, the contact point displacement-induced input f_{s1} can be identified.

2.2. Drive-by bridge modal identification

The proposed method is based on the fact that the ratio of a specific order mode shape value at any two locations is constant at any time. Therefore, mode decomposition is conducted using the identified contact point responses to separate the mode components. For this purpose, empirical mode decomposition (EMD), variational mode decomposition (VMD), or a band-pass filter can be used to extract the signal component corresponding to a specific mode. For the EMD and VMD-based methods, the number of intrinsic mode functions (IMFs) should be manually tuned according to the frequency distribution of the contact point vibration responses, which may be affected by external excitation. Since the proposed drive-by modal identification method is developed towards using multiple vehicle trips under operational conditions, the

external excitation may not be stationary. Therefore, band-pass filter-based signal decomposition is more robust than the EMD and VMD-based methods for this study. The bridge natural frequency needs to be identified from the drive-by measurement to specify the passband frequencies. Cross-spectrum estimation is proven to be able to amplify the bridge's natural frequency while suppressing other noise-relevant frequency components [17]. The cross-spectrum calculation is expressed as

$$G_{y_i y_j}(f) = \lim_{T\to\infty}\frac{2}{T}E[X^*(f,T)Y(f,T)] \tag{14}$$

where $G_{y_i y_j}$ represents the cross-spectral density function of the vehicle axle responses y_i and y_j measured from two adjacent vehicles. $X^*(f,T)$ and $Y(f,T)$ are the finite Fourier transforms of y_i and y_j. $E[\bullet]$, and asterisk * represent the mathematical expectation operator and complex conjugate, respectively.

According to Refs. [13,14], the analytical solution of the contact point response is dominated by the driving frequency $2n\pi v/L$ and the two shifted frequencies of the bridge. The appearance of the left-and right-shifted frequencies can be regarded as a type of Doppler effect due to the relative motion between the observer (vehicle) and vibration source (bridge). For example, a vehicle with a constant speed v crosses a bridge of length L, and the shifted frequencies corresponding to the *n-th* bridge mode are $\omega_{bn} - n\pi v/L$ and $\omega_{bn} + n\pi v/L$, respectively. To ensure that the bridge mode responses can be fully separated, the lower and upper cut-off frequencies for the *n-th* bridge mode are set as $f_L^n = \omega_{bn} - n\pi v/L$ and $f_H^n = \omega_{bn} + n\pi v/L$, respectively. The vibration response component corresponding to the *nth* mode is given as

$$y_{obs}^n = bandpass\left(y_{obs}, f_L^n, f_H^n\right) \tag{15}$$

According to the modal superposition principle, y_{obs}^n can also be expressed as

$$y_{obs}^n(x,t) = \xi_n(t)\phi_n(x) \tag{16}$$

Supposing that there are two moving sensors on the bridge at the time instant t, as shown in Fig. 4, the modal component response ratio between $y_{obs}^n(x_i,t)$ and $y_{obs}^n(x_j,t)$ is

$$\frac{y_{obs}^n(x_i,t)}{y_{obs}^n(x_j,t)} = \frac{\xi_n(t)\phi_n(x_i)}{\xi_n(t)\phi_n(x_j)} = \frac{\phi_n(x_i)}{\phi_n(x_j)} \tag{17}$$

where x_i and x_j represent the locations of the two moving sensors. Eq. (17) shows that the mode component response ratio between two points is equal to the mode shape value ratio independent of time. Eq. (17) can be rewritten as follows:

$$y_{obs}^n(x_i,t)\phi_n(x_j) - y_{obs}^n(x_j,t)\phi_n(x_i) = 0 \tag{18}$$

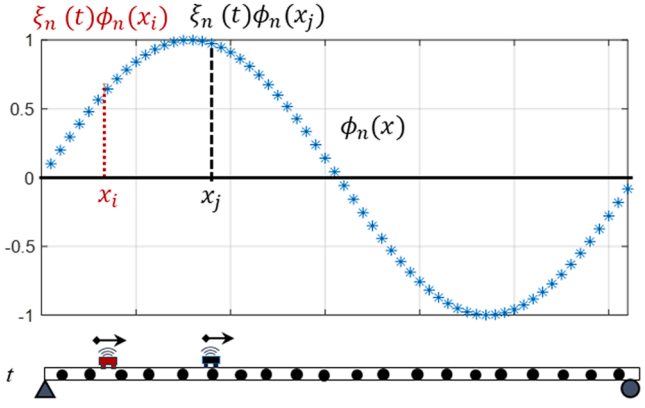

Fig. 4. Concept of mode shape value ratio between two contact points.

Using Eq. (18), it is possible to identify the bridge mode shape when at least two moving sensors are present on the bridge. Owing to the continuity of the bridge deflection curve along the longitudinal direction, the bridge mode shape should be globally smooth even if local stiffness reduction occurs. Therefore, the smoothness of the mode shape can be used as a physical-informed term of the objective function to assist in bridge mode shape identification. The following two objective loss functions are developed based on the above descriptions as

$$Loss = min\left\{\lambda\|\sum_{t=0}^{L/v} y_{obs}^n(x_i,t)\phi_n(x_j) - y_{obs}^n(x_j,t)\phi_n(x_i)\|_2 + (1-\lambda)\|\dot{\phi}_n\|_2\right\}$$

$$s.t.\begin{cases}\|\phi_n\|_2 = 1;\\ \phi_n(DoF_{support}) = 0.\end{cases} \tag{19}$$

where λ represents the weight of the error-related objective function. The *n-th* mode shape ϕ_n is variable to be optimized. $\dot{\phi}_n$ denotes the finite difference of the *n-th* mode shape ϕ_n, which is used to quantify the mode shape smoothness, $\|\bullet\|_2$ and $DoF_{support}$ represent the L2 norm and DOF at the bridge supports. The norm of the mode shape is constrained to 1. As indicated in Eq. (18)–(19), the spatial-resolution of *n-th* mode shape $\phi_n(x_i)$ can be up to v/f_s, which is much denser than the traditional SHM system with a fixed sensor network. v and f_s represent vehicle speed and sampling rate, respectively. For the multi-objective optimisation problem presented in Eq. (19), the Pareto front graph can be used to efficiently determine the weight coefficient λ and is thus employed in this study [36,37]. Eq. (19) is solved using the MATLAB Optimization Toolbox in-built function 'fmincon'.

In this study, a novel drive-by bridge mode shape identification framework, as shown in Fig. 5, incorporating crowdsensing to alleviate road roughness and measurement noise-induced uncertainties is developed. There are several advantages of the proposed approach with respect to existing representative studies: (i) the number of vehicles required to be present at the bridge at any given time is much less than that in the matrix completion-based method; (ii) since the mode shape is identified from time domain responses instead of using frequency domain information, it is better suited to normal traffic speed with low vehicle–bridge interaction time; (iii) since the ratio of the mode shape value at two particular locations is not affected by the external input, the proposed drive-by modal identification method is robust to external excitations; and (iv) the proposed method can be incorporated into the

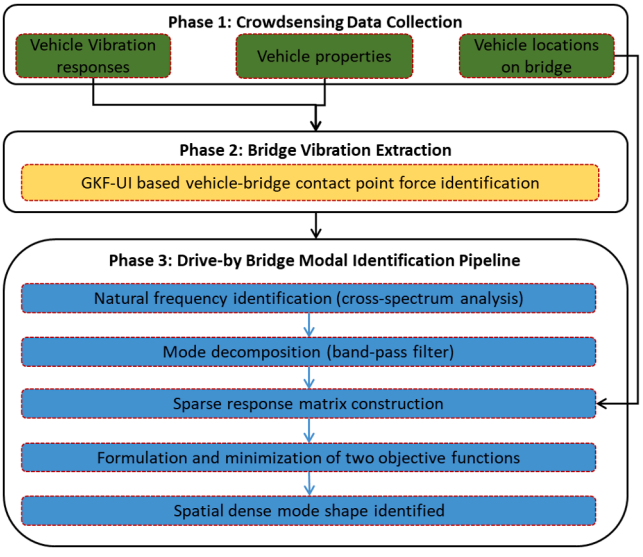

Fig. 5. Process flow of the proposed drive-by bridge modal identification method.

crowdsensing technique, and this study verifies that crowdsensing could alleviate road roughness and the measurement effect on modal identification of bridges under traffic loads.

3. Numerical validation and influencing factor analysis

Numerical simulations are conducted to validate the performance of the proposed modal identification method for bridges subjected to traffic. The influences of factors such as road roughness, measurement noise, vehicle speed, bridge type, and span on the modal identification accuracy are analysed. In addition, the performance of crowdsensing in alleviating the uncertainties induced by the above-mentioned influential factors is investigated and discussed here.

3.1. Numerical model setup

The vehicle-bridge interaction system is illustrated in Fig. 6. The bridge sub-system parameters are listed as follows: reinforced concrete equivalent Young's modulus $E = 3.5 \times 10^{10}\text{N/m}^2$; material density 2400 kg/m^3; bridge span $L = 60$ m; bridge cross-section with a width of 6 m and a height of 1.5 m. The bridge modal damping ratio is taken to be 1% for the first three modes of interest. The bridge model is discretised into 100 elements with two DOFs per node. The first three order bridge frequencies are obtained as 0.7215 Hz, 2.8861 Hz, and 6.4937 Hz. The vehicle and bridge mechanical parameters are adopted with modifications from Ref. [28]. For more realistic simulation of the mobile crowdsensing scenarios, the vehicle parameters corresponding to each trip are randomly regenerated according to the normal distribution. In particular, the mean values and standard deviations of vehicle sub-system parameters are listed in Table 1.

The quarter-car model shown in Fig. 6 can capture many important vehicle–bridge interaction characteristics and is commonly used to validate drive-by methods. The first and second mode frequencies of the quarter-car model with all parameters fixed at its mean value (shown in Table 1) are calculated as 2.2138 Hz and 16.9233 Hz, respectively.

Three quarter-car models (as presented in Fig. 6) are used to scan three contact point responses. A similar consideration of vehicle model can be found in Ref. [28]. The distances between the first two and last two quarter-car models are $d_{s1} = 2$ m and $d_{s2} = 4$ m, respectively. As discussed in Section 2, the proposed mode shape identification method requires at least two contact point responses. In this numerical study, each pair of the three quarter-car models could be used to calculate the mode shape value ratio. Therefore, the overall number of mode shape value ratios generated by the three quarter-car models is approximately three times that produced by the two quarter-car models. The interval distances d_{s1}, d_{s2} and vehicle speed are assumed to be constant. However, the proposed method can also be applied to the scenarios with varying distances and nonuniform speeds. The dynamic interaction between the vehicle and bridge subsystems is coupled at the tire contact point via contact point displacement. Three vehicle body mass acceleration responses $\boldsymbol{a}_1$, $\boldsymbol{a}_2$, and $\boldsymbol{a}_3$ are collected with a sampling rate of 1000 Hz and used as the input for the GKF-UI-based method to identify the contact point response. An approach road with a length of 10 m is considered at both ends of the bridge. The vehicle starts from the approach road to ensure that steady-state responses can be obtained during the vehicle–bridge interaction stage. It is noted that the mass ratio of the vehicle to bridge beam is assumed to be small ($m_v \ll \overline{m}L$), so that the bridge dynamic motion obeys the linear elastic theory and satisfies the mode superposition principle. To simulate a more realistic bridge operational conditions, ambient random excitations with a standard deviation of 0.05 g are applied to the bridge model.

Table 1
Vehicle sub-system parameters.

Parameters	Mean value μ	Standard deviation σ
vehicle body mass m_b (kg)	2000	100
vehicle tyre mass m_s(kg)	200	10
vehicle body stiffness k_b (N/m)	5×10^5	2.5×10^4
vehicle tyre stiffness k_s (N/m)	1.76×10^6	8.56×10^4
vehicle body damping c_b(N·s/m)	1×10^4	500
vehicle tyre damping c_s (N·s/m)	0	0

Road roughness is an important source of dynamic excitation in road traffic that affects drive-by SHM performance. In this study, five road roughness surface classes, namely class A (very good), B (good), C (medium), D (poor) and E (very poor), are generated according to the power densities in ISO-8608. Ref. [26] provides a detailed description of the roughness generation. Owing to the difficulty in controlling the vehicles passing the bridge on the same path during each trip, the road roughness corresponding to each road class is regenerated for each trip. Unless otherwise specified, the measurement noise is taken to be 1%, road class to be A, and vehicle speed $v = 10$ m/s (36 km/h) to generate the drive-by measurements.

In the numerical validations in this study, the speed and distance of two adjacent vehicles are assumed to be constant. This assumption can be satisfied by considering each axle of a multi-axle vehicle as a measurement node with a fixed distance between two axles, or connecting two vehicles together. However, it should be noted that the proposed method could also be applied to scenarios with varying distances and nonuniform speeds. As shown in Eq. (19), the two objective loss functions can be established when the locations of two measurement positions x_i and x_j are given. As illustrated in Fig. 1(b), the sparse matrices can be generated from the vehicles as moving sensors with different velocities.

3.2. Bridge mode shape identification using the proposed method

This section describes the procedure of the proposed drive-by bridge modal identification framework, given the numerically generated three-quarter-vehicle body acceleration responses $\boldsymbol{a}_1$,$\boldsymbol{a}_2$ and $\boldsymbol{a}_3$. Fig. 7 shows the identified contact point displacements for the three vehicle models using the GKF-UI-based method, which agree well with the ground truth results extracted from FE model. The normalised root-mean-square error (NRMSE) [38] of all three quarter-vehicle models are under 0.3%. As the green background colour indicates, the first quarter-car model is present on the bridge between 0.4 and 6.4 s (corresponding to samples 401–6400). The data corresponding to at least two vehicles simultaneously on the bridge can be used to calculate the mode shape ratio defined in Eq. (17). Therefore, for contact point pairs 1–2, 1–3, and 2–3,

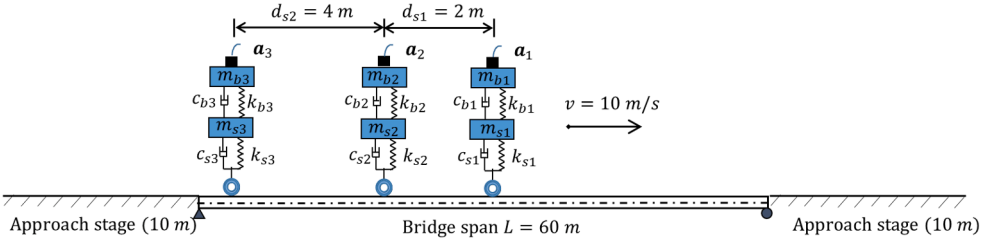

Fig. 6. Three quarter-car models travelling over bridge.

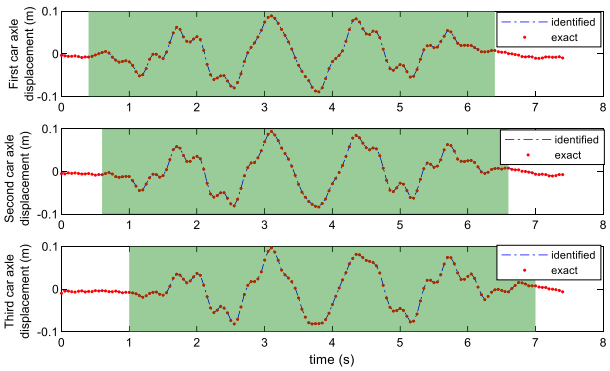

Fig. 7. Contact point displacement identified by the GKF-UI-based method. The NRMSE of the first, second, and third contact point displacements are 0.12%, 0.24% and 0.16%, respectively. The interval with the green background represents the duration the axle is on the bridge. (For interpretation of the references to colour in this figure legend, the reader is referred to the web version of this article.)

the number of equations that can be used to construct Eq. (19) are 5800, 5400, and 5600, respectively. The number of unknown variables in $\phi_n(x)$ depends on the spatial density of the required mode shapes. In general, for a bridge with a span of 60 m, 101 variables uniformly distributed along the longitudinal direction is a dense enough distribution to locate the local structural damage with metre-level resolution. Therefore, one trip of the three quarter-car models passing over the bridge will provide 16,800 equations for Eq. (19) to optimise the mode-shape solution with 101 unknown variables. The first-and second-mode components (Fig. 8) are extracted from the identified contact point responses using a bandpass filter.

The mode components are then used to construct a loss function with two objectives, as described in Eq. (19). To use Eq. (19), it is important to determine the weight coefficient λ for each objective function. In this study, a Pareto front graph is employed to satisfy this purpose. A series of 150 weight coefficients within the interval $[10^{-5} \leq \lambda \leq 0.2]$ are successively used to solve Eq. (19). The weight coefficients range is determined based on trial calculation. The computations are performed on a desktop with an Intel(R) Core (TM) i7-7700 CPU (3.6 GHz) and 16 GB RAM. For numerical case 1, the computational time of iterating over 150 weight coefficients λ to generate the Pareto front graph and obtain the optimal solution is about 745 s. The maximum number of iterations for each λ is 10^4. Fig. 9 shows a Pareto front graph, with each point representing the optimal solution to Eq. (19) with a specific λ. The x- and y-axes denote the second term of the objective function in the optimization (mode shape smoothness) and the first term of the objective function (mode shape identification error), respectively. The bottom left and upper right regions of the Pareto front graph represent the infeasible and feasible solutions, respectively. The optimal weight coefficient can be selected to maintain a balance between the modal identification accuracy and mode shape smoothness. Overfitting may occur when the minimum of the first objective is pursued excessively. In this study, $\lambda = 0.00476$ is selected for both the first-and second-mode shape identification. The first two mode shape identification results using data from a one-trip measurement are presented in Fig. 10 and Fig. 11, respectively. The MAC values between the exact and identified first and second mode shapes are 0.9993 and 0.9987, respectively. The estimated first and second mode shapes are consistent with the exact bridge mode shape, as indicated by the modal assurance criteria (MAC) value. In addition, both terms in the defined objective function converge quickly to relatively small values after 200 iterations. It is important to note that data from only one trip are used in this case to obtain desirable mode shape identification results, and this method substantially outperforms the existing matrix completion-based method presented in Ref. [31] by using data measured from a large number of vehicles.

3.3. Influencing factors and crowdsensing

Results of previous studies indicate that the road profile, measurement noise, and vehicle speed adversely affect the identification accuracy of bridge modal properties from vehicle responses. These factors are examined in this section to evaluate the robustness of the proposed method. Crowdsensing is introduced to improve the performance in relation to these factors.

3.3.1. Road roughness and expansion joint

Fig. 12 shows the MAC values of the identified mode shapes subjected to road roughness classes A to E. Crowdsensing is incorporated in the data collection using data from 1, 5, 10, 20, and 50 independent trips as the input to Eq. (19). This is different from the matrix completion-based modal identification method, which requires a population of vehicles to be simultaneously present on the bridge. The results presented in Fig. 12 are the average of 10 repeated simulations with randomly generated road surface roughness profiles for each trip to minimise the errors in modal identification. Fig. 12 shows that the overall MAC value significantly decreases with deteriorating road surface conditions when using single-trip data. However, the modal identification accuracy improves upon introducing crowdsensing data. In particular, the MAC values of the first and second modes are higher than 0.988 and 0.972, respectively, when data collected over 20 trips on road class D are used by the proposed mode shape identification method. The corresponding first two mode shape identification results are presented in Fig. 13. However, the MAC value for the first two mode shapes identified assuming road class E are less than 0.92 even when data from 50 trips are used. This is because the contact point displacement is a combination

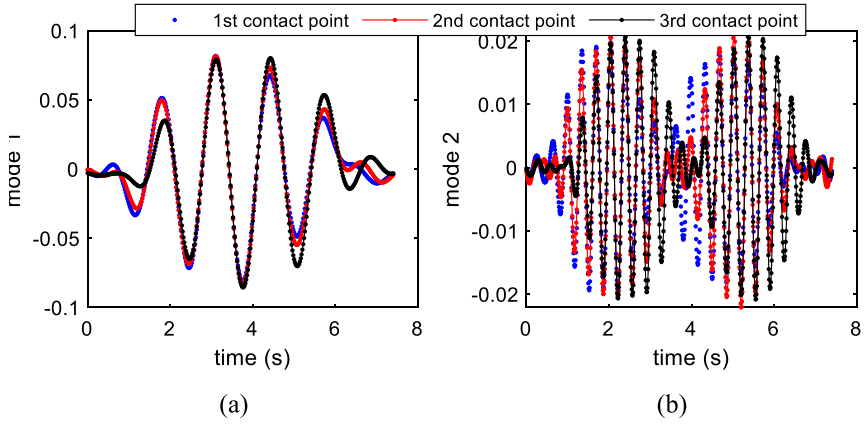

Fig. 8. (a) First and (b) second mode response component extracted using bandpass filter.

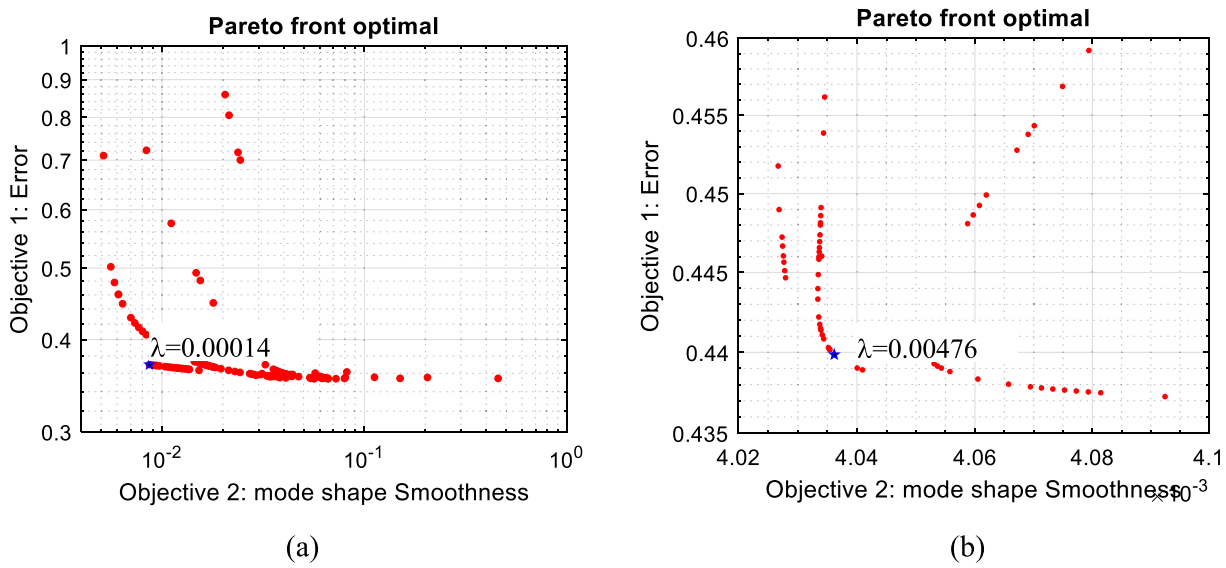

Fig. 9. Pareto front graphs of: (a) the first; and (b) the second mode component.

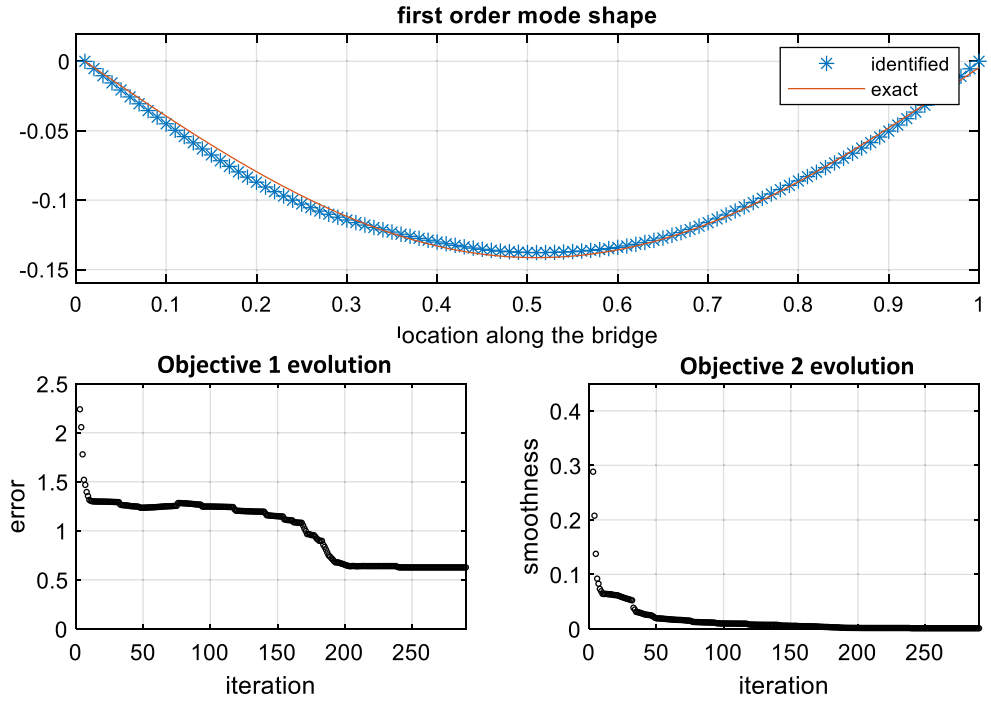

Fig. 10. First mode shape identification results and evolutions of objectives 1 and 2 over iterations.

of bridge dynamic displacement and road roughness. Therefore, the bridge mode shape identification accuracy can be substantially affected by the road roughness. The mode shape identification accuracy might be improved by using heavier vehicle to increase the moving-load induced bridge dynamic displacement or introducing advanced signal processing technique to eliminate road roughness effect. The results presented in Fig. 12 also verified that the proposed method is also applicable even if the road roughness corresponding to each trip is different, which is an important merit for the field application.

Considering that the effect of expansion joint on a real bridge on vehicle vibration may differ from the road roughness generated from the standard ISO-8608, the effect of the expansion joint is investigated to examine the robustness of the developed method. An expansion joint with a width of 0.1 m and depth of 3 cm was considered at a position of 20 m from the left end of the bridge. Fig. 14(a) shows the combination of randomly generated road roughness (class A) and expansion joints. The vehicle body vibration responses when passing the bridge with the expansion joint are presented in Fig. 14 (b), which shows that the three quarter-vehicle responses are highly sensitive to the expansion joint. Similarly, three spikes are present in the identified contact point responses, as shown in Fig. 14 (c). In the frequency domain, the abrupt change in the contact point force induced by the expansion joint is mainly distributed in the high-frequency region. When a band-pass filter is applied, no spikes are seen in the extracted first-and second-mode response components, as shown in Fig. 14(d–e). Finally, the mode shape identification results obtained using the single-trip data taking into

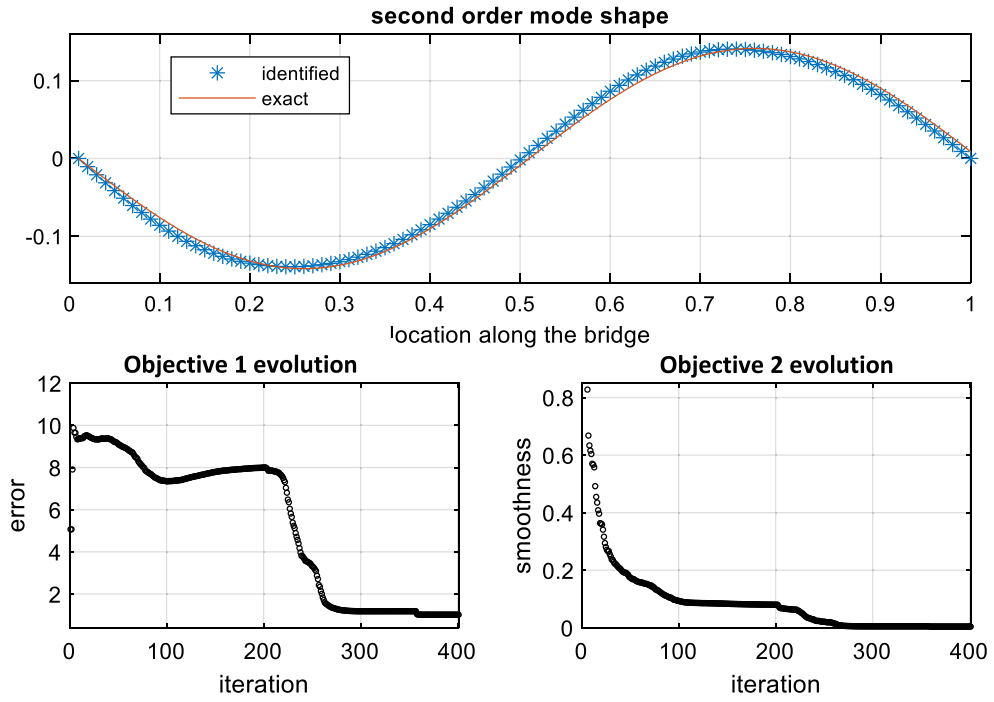

Fig. 11. Second mode shape identification results and evolution of objectives 1 and 2 over iterations.

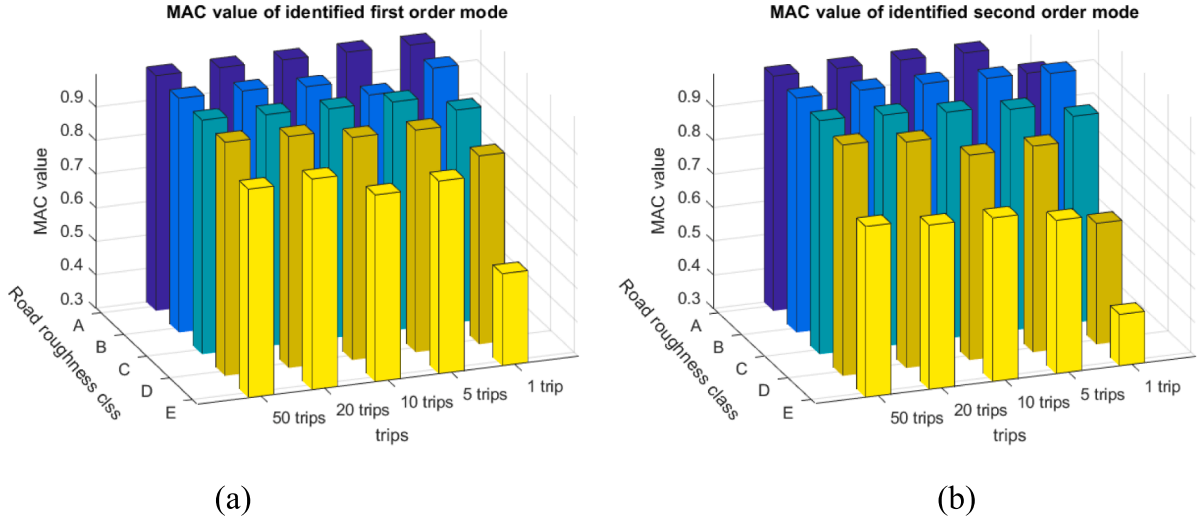

Fig. 12. MAC values of identified (a) first mode and (b) second mode subjected to different road roughness conditions.

account the expansion joint are presented in Fig. 15. The identified mode shapes agree well with the ground truth, and the corresponding MAC values of the first and second mode shapes are 0.9996 and 0.9982, respectively.

3.3.2. *Measurement noise effects*

To investigate the influence of measurement noise, five levels (1, 2, 3, 4, and 5%) of white noises are respectively added to the vehicle body acceleration responses. Mode shapes are identified by repeating the procedure shown in Fig. 5. The MAC values of the identified mode shapes under different noise levels using data from different numbers of trips are presented in Fig. 16. The effects of measurement noise are similar to those of the road roughness. The noise effects are significantly suppressed when data from more numbers of trips are used. In particular, the MAC values of the first and second mode shapes are higher than 99% when data from 20 trips with 4% measurement noise are used. The corresponding identification results for the first two mode shapes are presented in Fig. 17.

3.3.3. *Vehicle speed effects*

As mentioned in Section 2.2, the lower and upper cut-off frequencies of the bandpass filter are given as $f_L^n = \omega_{bn} - n\pi v/L$ and $f_H^n = \omega_{bn} + n\pi v/L$, respectively. The first and second natural frequencies of simulated bridge are approximately 0.72 Hz and 2.88 Hz, respectively. Therefore, the upper cut-off frequencies of the first mode and lower cut-off frequency of the second mode overlap when the vehicle speed exceeds 13.78 m/s. To investigate the influence of vehicle speed on the mode shape identification performance by using the proposed method, a series of vehicle speeds, namely, 6 m/s (21.6 km/h), 8 m/s (28.8 km/h), 10 m/s (36 km/h), and 12 m/s (43.2 km/h) are considered. The MAC

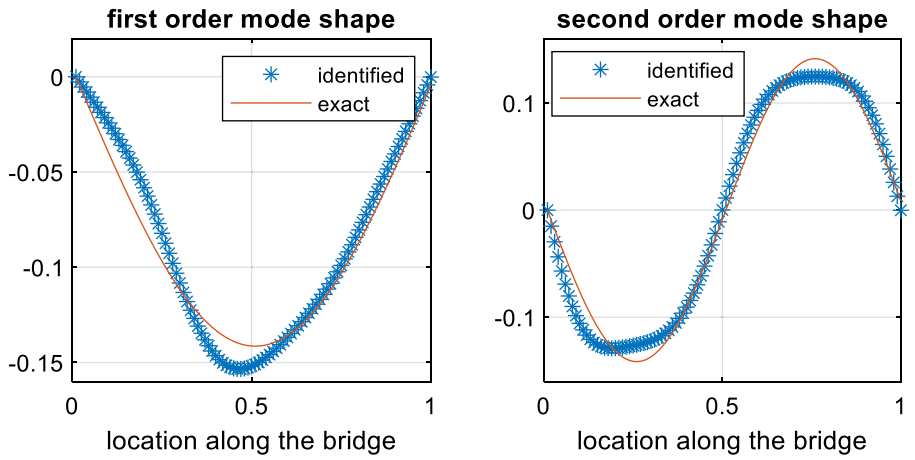

Fig. 13. Identified (a) first mode and (b) second mode with data collected over 20 trips on road with roughness class D.

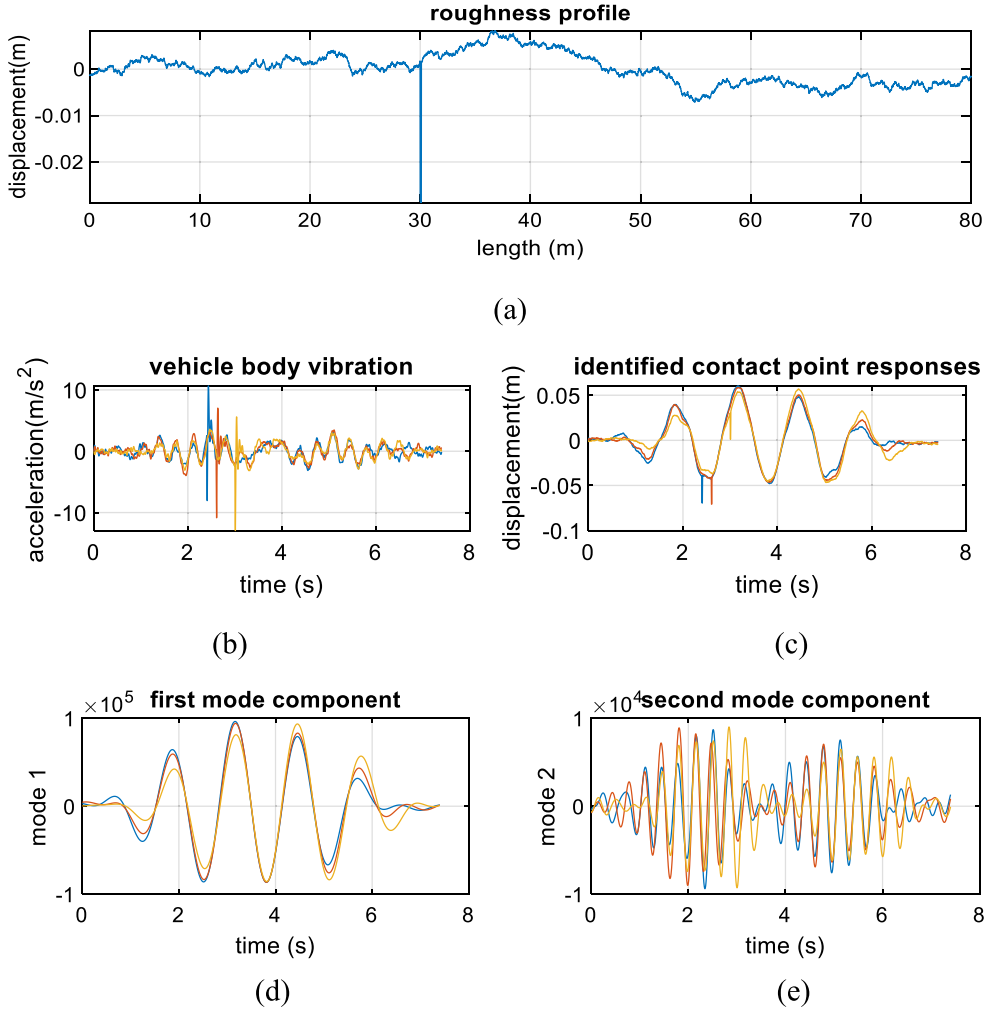

Fig. 14. (a) Road surface roughness with expansion joint, (b) vehicle body vibration responses, (c) identified contact point responses, (d) first mode response component, and (e) second mode response component.

value declines slightly as the vehicle speed increases (Fig. 18). The vehicle speed mainly affects the vehicle–bridge interaction time when it passes the bridge. Since the proposed method identifies the bridge mode shape directly from time domain responses instead of using frequency domain information, the proposed method is more robust to vehicle speed than the existing frequency domain-based method. However, in practice, the vehicle–bridge interaction will be more complicated than considered here owing to the high-speed vehicle bump effect on the bridge [39], which was not explicitly considered in this study.

3.3.4. *Bridge type and span*

In the previous section, a simply supported uniform cross-section bridge with a span of 60 m is considered to investigate the feasibility and advantages of the proposed method. In this section, a three-span

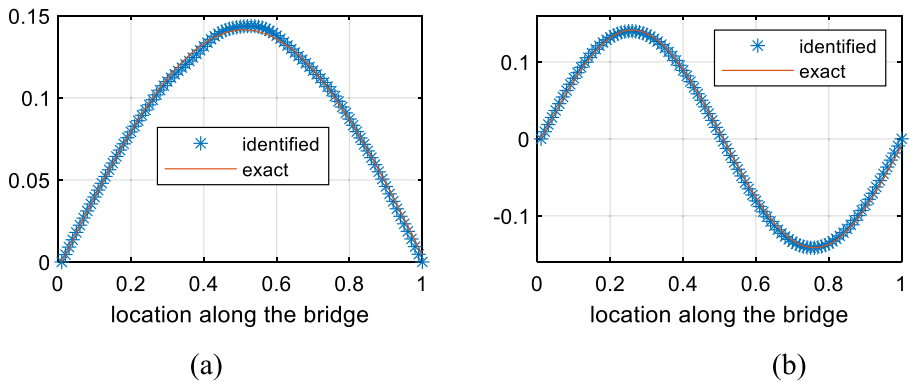

Fig. 15. Identified (a) first mode and (b) second mode considering the expansion joint.

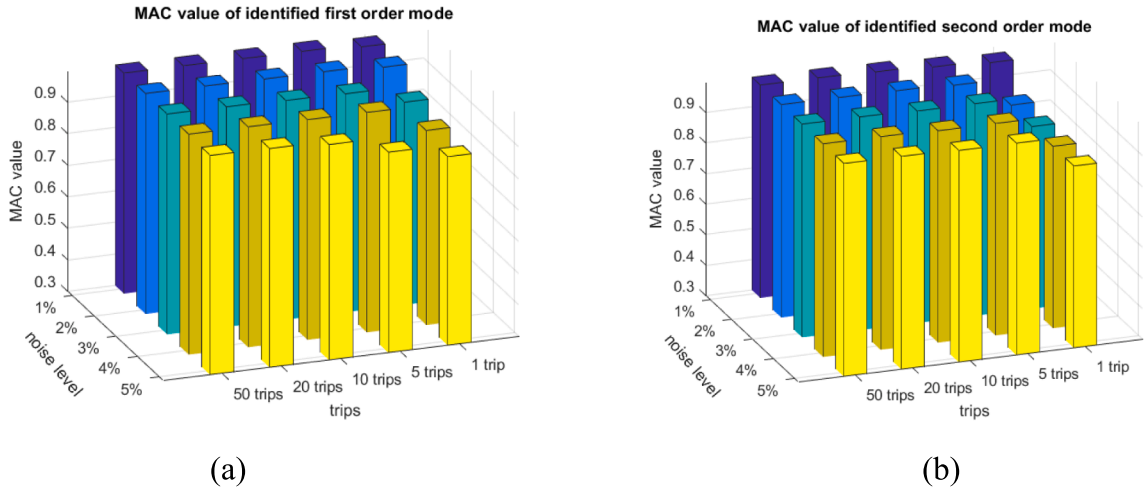

Fig. 16. MAC value of identified (a) first mode and (b) second mode with different measurement noise levels.

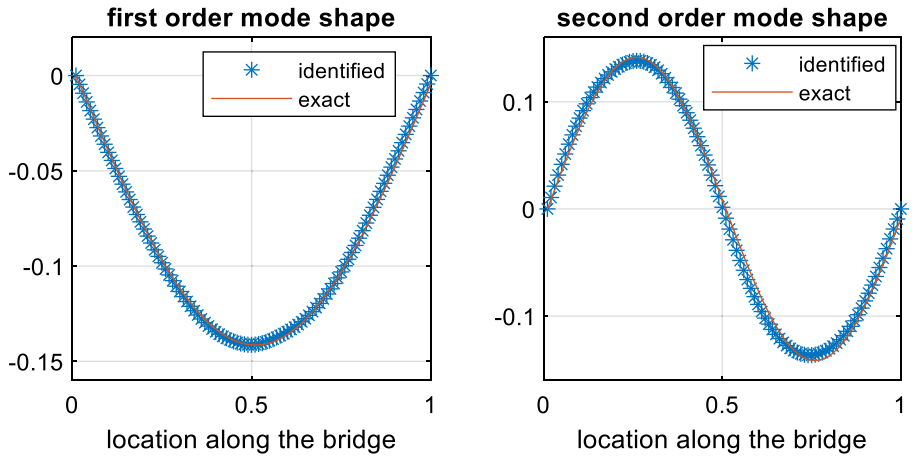

Fig. 17. Identified (a) first mode and (b) second mode with data from 20 trips polluted by 4% measurement noise.

continuous beam bridge (40 m + 60 m + 40 m) with varying cross sections is considered to demonstrate the application of the proposed method to more general bridge types and spans. The bridge model is divided into 140 elements of equal length. The height of the cross-section at the supports and mid-span are 2.6 and 1.6 m, respectively. The variation of cross-section from the supports to the mid-span section satisfies the quadratic curve. Other bridge model parameters are the same as those of the simply supported bridge, as shown in Fig. 6. The exact mode shapes are extracted from the FE model and will be used to compare with the model shape identified from the proposed method.

In the analysis presented in Section 3.1, three quarter-vehicle models are used to identify the bridge mode shape. However, the contact point responses measured from only three quarter-vehicle may not be sufficient to accurately identify the mode shape of a long-span bridge with multiple spans for the following reasons: (i) for long-span bridges, the mode shape value ratio between two contact points is approximately 1 if

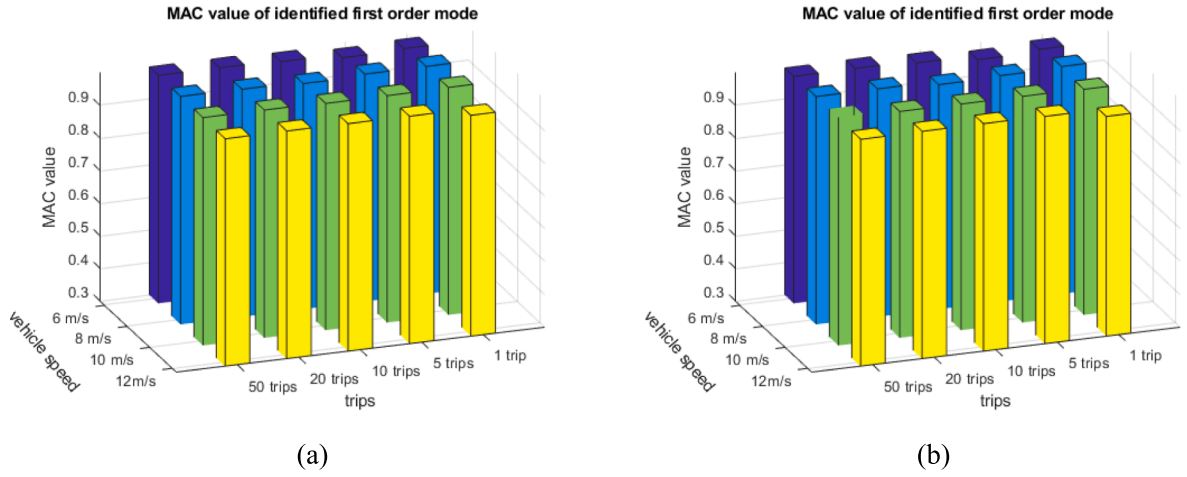

Fig. 18. MAC value of identified: (a) first mode and (b) second mode with different vehicle speeds.

the ratio between two contact points' distance and the bridge span length is small. Thus, the accuracy of the estimated mode shape is considerably affected by the measurement noise and road surface roughness; (ii) for a multi-span bridge, the data samples corresponding to two moving sensors on the adjacent span are important to accurately identify the relative mode shape amplitude of the two spans. However, because the distance between two moving sensors is much shorter than the bridge span, the data samples are insufficient. The performance of the proposed method for long-span bridges with multiple spans can be improved by using data from more vehicles simultaneously distributed on different spatial locations of the bridge. It is assumed that the data measured from six quarter-vehicles are available to identify the mode shape of the bridge, as illustrated in Fig. 19. The distance between the first three and last three quarter-vehicles is assumed to be 30 m. Other vehicle parameters are the same as those used in Section 3.1. The procedure is detailed in Fig. 5. As shown in Fig. 20, the weight coefficients of the first and second modes are determined as $\lambda = 0.00014$ and $\lambda = 0.0003$, respectively. The mode shape identification results of the first and second modes using data from one-trip are presented in Fig. 21 and Fig. 22, respectively. Both objectives of the first mode converge to a relatively small value after 150 iterations. The MAC values of the first and second mode shapes are 0.9987 and 0.9766, respectively. The numerical results verify that the proposed method is applicable to bridges with multiple spans and varying cross-sections, when data measured simultaneously from multiple vehicles are used. It should be noted that the in-situ time synchronisation of the data measured from multiple vehicles is important for the success of the proposed method, and this aspect is not explicitly discussed in this paper.

4. Large-scale bridge application

4.1. Experimental setup

In this section, a series of moving vehicle tests are conducted on a full-scale double-girder concrete footbridge located on the third floor of Building 215, Curtin University. As shown in Fig. 23(a), Building 215 is a three-storey steel–concrete composite building installed with a long-term SHM system, which is used as a benchmark platform. To validate the effectiveness and accuracy of the developed method, this study identifies the mode shape of the third-floor footbridge and compares it with the mode shape identified from a fixed sensor network. The length of the footbridge is approximately 11 m. Fig. 23(b) shows the placement of the fixed accelerometer and the vehicle's travel path during the drive-by test. As shown in Fig. 23 (c), four accelerometers were attached to the experimental vehicle model, two on the front and rear vehicle bodies and two on the front and rear axles. The vehicle is driven at the rear wheel by two servo motors, which greatly reduces the friction vibration induced by the stepper motor. The distance between the front and rear axle is 32.5 cm. Four mass blocks, as shown in Fig. 23 (d), are fixed on the vehicle body to simulate a different vehicle mass state. Five scenarios listed in Table 1, including two different vehicle masses and three vehicle speeds, are considered to validate the accuracy of the proposed method. For each scenario, the drive-by experimental test is repeated ten times to simulate crowdsensing data collection. Overall, data from 50 trips are collected. The sampling rate of installed accelerometers is set as 500 Hz. The weight coefficients of both objectives for each scenario are determined by the Pareto front graph and are listed in Table 2. Although a constant speed is set by the remote controller during each trip, the vehicle speed and travel path are not exactly the same. To make use of the crowdsensing measurements with different lengths of data points,

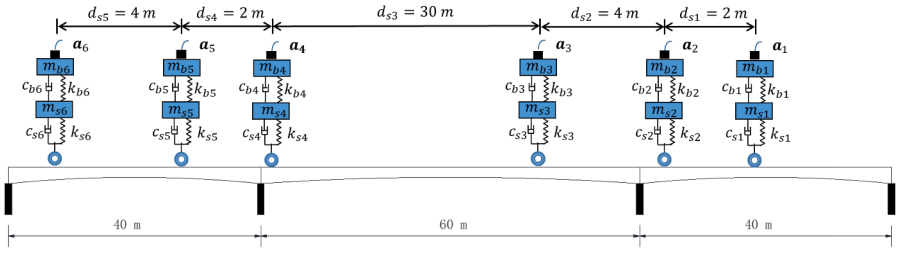

Fig. 19. Three-span continuous beam bridge model with variable cross-section.

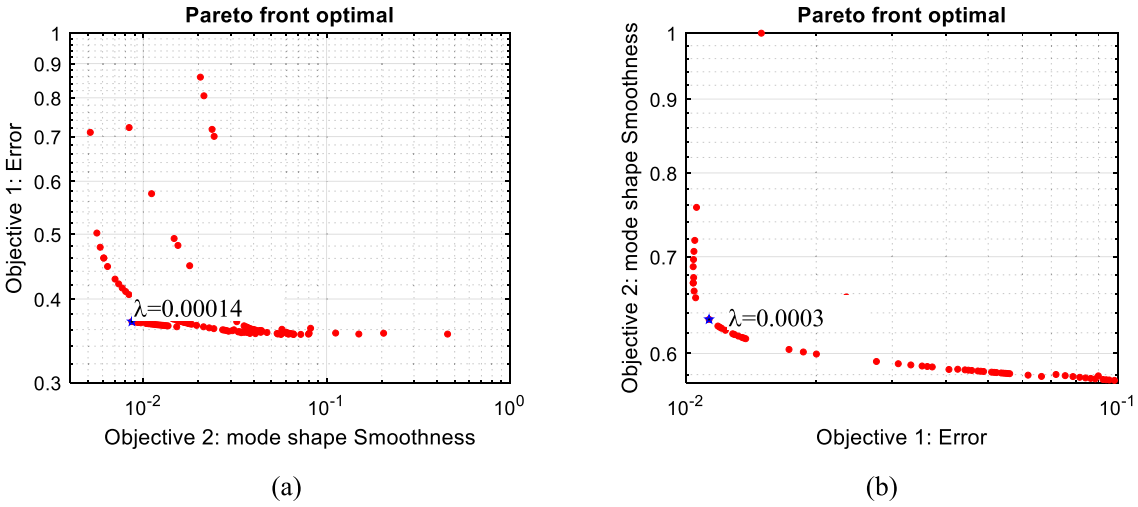

Fig. 20. (a) Pareto front graph of (a) first and (b) second mode components.

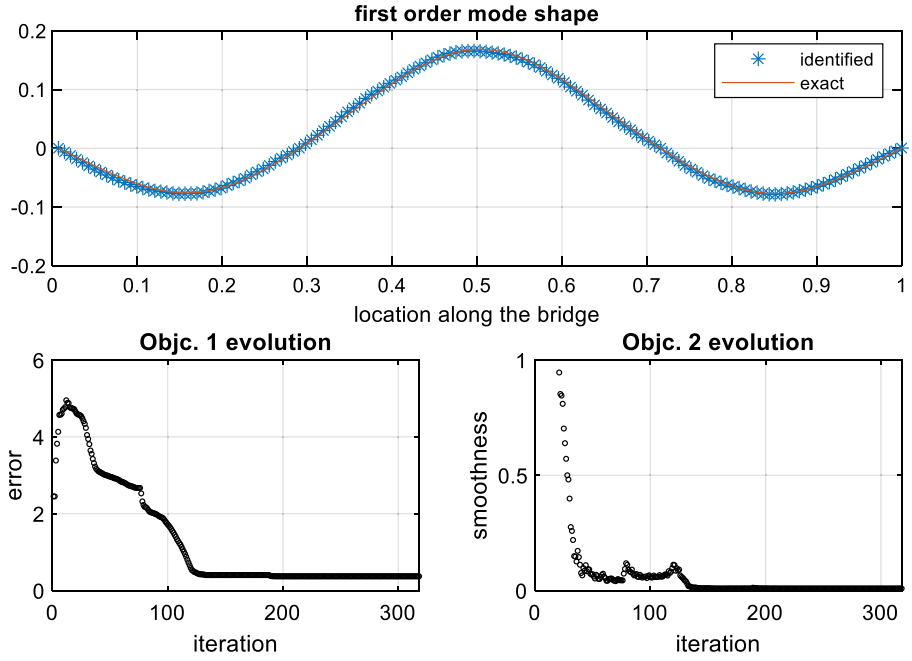

Fig. 21. First mode shape identification results and evolution of objectives 1 and 2 over iterations. The MAC between the exact and identified mode shape is 0.9987.

the signal repeatedly collected from each trip is resampled to the same length before conducting the proposed drive-by mode shape identification. The vehicle model used in the experimental tests is approximately rigid., The vehicle–bridge contact point displacements are completely transmitted to the axles and vehicle body [26,30]. The deformation of the tyre is negligible. However, the vertical dynamic displacement of moving vehicle is difficult to measure. Instead, only the acceleration response is available. In the measurement point, the frequency responses function between displacement and acceleration responses is $-\omega^2$ at any specific frequency component. As a result, the mode shape identified from acceleration responses and displacement responses is the same. In the experimental study, the axles acceleration responses are used to identify bridge mode shape by following the drive-by bridge mode shape identification procedure summarised in Phase 3, as shown in Fig. 5.

Since the vehicle mass (approximately 6 kg) is negligible compared to the mass of the full-scale bridge, additional pedestrian loads from a group of people walking on the bridge are applied during the test to excite the bridge. In particular, five people walk out and in the footbridge with a random pace to simulate the pedestrian load. The measured front and rear axle responses are then used to identify the bridge mode shapes. An example of responses for a vehicle moving at a speed of 0.15 m/s is shown in Fig. 24. Fig. 24(a) and Fig. 24(b) present the acceleration responses of the front and rear axles when passing the bridge. The first mode frequency (close to 7 Hz) can be easily identified from the cross-spectrum of both axle responses presented in Fig. 24(c). The high-order mode of the footbridge is not excited under pedestrian loads. The mode responses as shown in Fig. 24(d) corresponding to frequency range from 6.85 to 7.15 Hz is extracted by using the bandpass filter. As shown in Fig. 24(d), the amplitude of the front axle responses is higher than that of the rear axle when the vehicle passes the first half of the bridge and vice versa. This is because the first mode shape value is relatively large in the mid-span. This phenomenon indirectly confirms that the response corresponding to the first mode component is correctly separated through the band-pass filter.

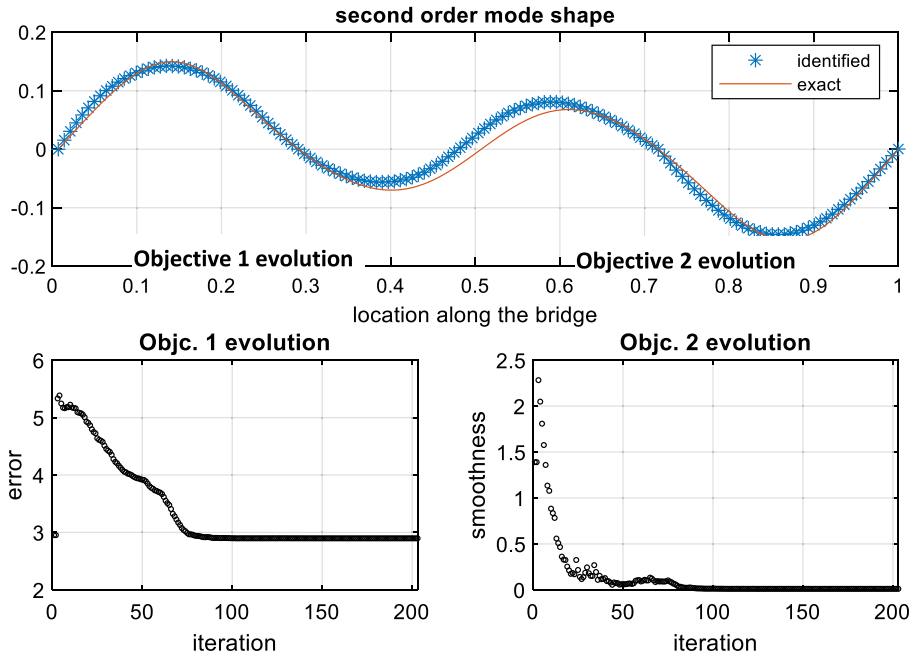

Fig. 22. Second mode shape identification results and evolution of objectives 1 and 2 over iterations. The MAC between the exact and identified mode shape is 0.9766.

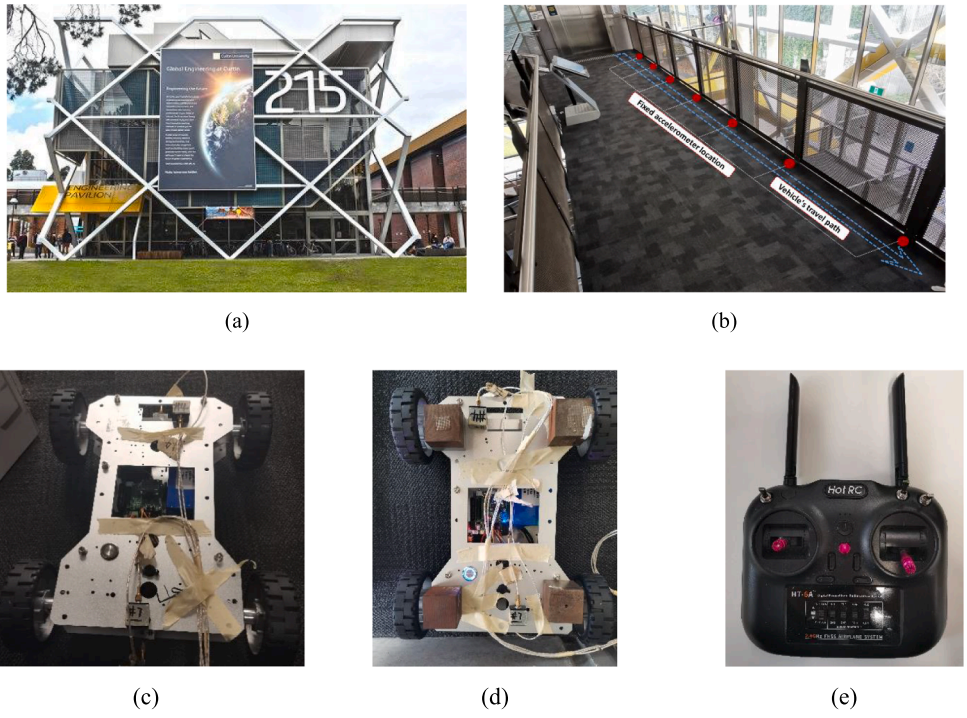

Fig. 23. (a) Elevation view of Building 215 (b) fixed sensor placement and vehicle's travel path on third floor footbridge, (c) in-house made vehicle model for this study, (d) vehicle model with four added mass blocks, and (e) vehicle remote control unit.

4.2. Dense spatial-resolution mode shape identification result analysis

The mode shape of each scenario listed in Table 2 is identified through the procedures detailed in Phase 3 of Fig. 5. Fig. 25 shows the first mode shape identification result for Scenario #3 and the evolutions of objectives 1 and 2 during the iteration process. As shown in Fig. 25(a), the mode shape identified from the proposed method using crowd-sensing measurement agrees well with that from the fixed sensor network. The FDD-based method is used to obtain the mode shape from

Table 2
Experimental test scenarios and description of parameters.

Scenario	#1	#2	#3	#4	#5
Vehicle speed	0.15 m/s	0.15 m/s	0.3 m/s	0.3 m/s	0.36 m/s
Add mass block	No	Yes	No	Yes	Yes
Weight coefficient λ	0.135	0.075	0.065	0.24	0.165
Number of repeated trips	10 trips	10 trips	10 trips	10 trips	10 trips

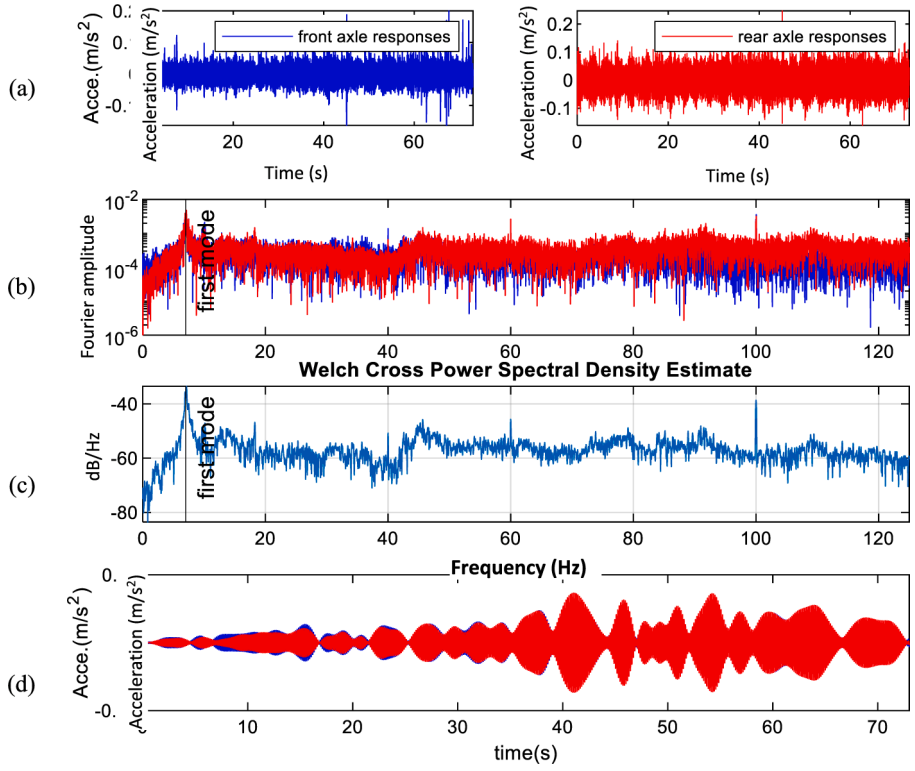

Fig. 24. (a) Front and rear axle response time series, (b) Fourier spectrum of front and rear axle responses, (c) cross power spectrum, and (d) extracted first mode response component of front and rear axles. The blue and red line represent the front and rear axle responses, respectively.

the fixed sensor network. Both objectives decrease monotonically and finally converge after 200 iterations. The MAC value between the mode shapes identified from the moving sensor and fixed sensor is 0.9972, implying that the proposed method can be a potential alternative for accurately identifying the bridge structure mode shape. In comparison, the MAC values corresponding to all five scenarios are presented in Fig. 26. Overall, the MAC values are higher than 0.98 for all five scenarios. It is also observed that the mode shape identified from the proposed method is much denser than that identified from fixed sensor network. The experimental results indicate that the variation in vehicle speed and vehicle mass has minimum influence on the modal identification accuracy of the proposed method. The results also demonstrate that the proposed approach can be used to scenarios with different vehicle parameters and road roughness conditions.

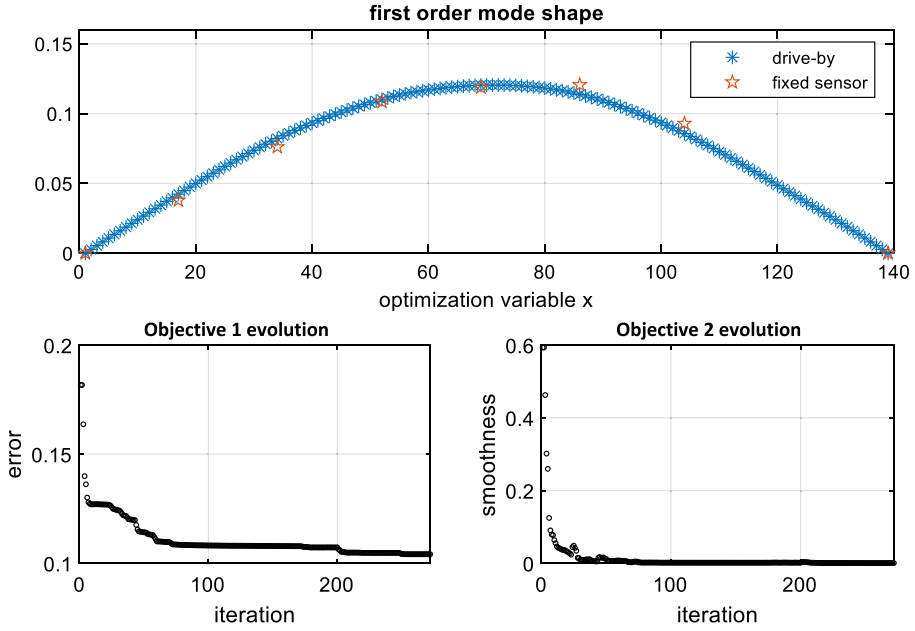

Fig. 25. First mode shape identification result and evolution of objectives 1 and 2 over iterations. There was no added mass and the vehicle speed was v_2. The MAC between the exact and identified mode shape is 0.9972.

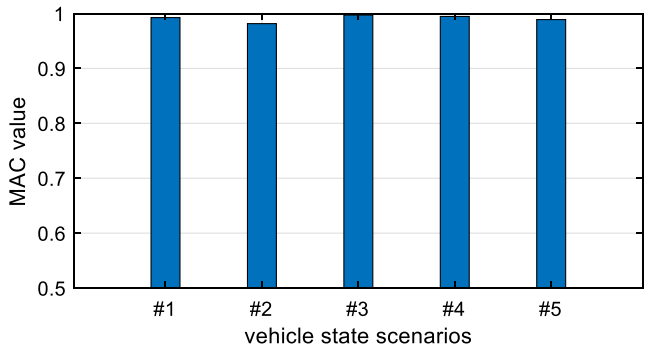

Fig. 26. MAC value of five vehicle state scenarios.

5. Conclusions

This paper proposes a crowdsensing framework to indirectly identify bridge mode shapes from vibration responses of vehicles moving on the bridge. Results of numerical studies on a 60 m long simply supported bridge demonstrate that the proposed method is effective and robust under a wide range of vehicle speeds, road roughness, and measurement noise levels. The uncertainties induced by pavement roughness and sensor noise could be significantly suppressed by incorporating crowdsensing during the signal collection process. Overall, the MAC values of the first and second mode shapes are greater than 98% when data from 20 trips smeared with 4% measurement noise under road roughness class D are used. The numerical validation is also extended to the modal identification of a continuous three span bridge, and the natural frequencies and mode shapes can also be identified accurately. A series of drive-by tests with different vehicle masses and speeds are conducted on a full-scale footbridge. The experimental results verify the practicality of the proposed method. Overall, the MAC values between the mode shape identified by the proposed method and the fixed sensor network are higher than 0.98 for all the considered vehicle scenarios. The spatial resolution of the mode shape identified from the proposed method is higher than that from the traditional fixed sensor network. Thus, the proposed method can be potentially incorporated with mode shape-based damage features to locate structural damage. To the best of our knowledge, this is the first study to identify the mode shape of a full-scale structure by using drive-by measurements.

There are several limitations that need to be addressed before the practical implementation of the proposed mobile crowdsensing SHM framework. Firstly, there is a need to address how to synchronize the data collected from various vehicles on the bridge in practical applications. Secondly, the complexity of the suspension system in commercial vehicles is significantly higher than the vehicle model considered in this study, which presents a challenge in identifying the vehicle-bridge contact point responses. For future practical implementations of the proposed approach, the applicability of the proposed method by using commercial vehicles and signal synchronisation between multiple vehicles require further investigations. It is noted that other factors, such as the frequency ratio between the vehicle and the bridge may also affect the drive-by modal identification. This has been investigated in previous studies and it is not a main focus of this study and could be investigated in future work. It might be difficult to keep the velocities of different vehicles consistent during the whole period in a test. Further studies can be conducted to investigate the case with varying vehicle velocities when the vehicles are crossing the bridge.

CRediT authorship contribution statement

Zhen Peng: Conceptualization, Methodology, Validation, Formal analysis, Investigation, Data curation, Writing – original draft, Visualization. **Jun Li:** Conceptualization, Methodology, Investigation, Writing – review & editing, Supervision, Funding acquisition. **Hong Hao:** Conceptualization, Methodology, Investigation, Writing – review & editing, Supervision. **Ning Yang:** Methodology, Validation, Formal analysis, Investigation.

Declaration of Competing Interest

The authors declare that they have no known competing financial interests or personal relationships that could have appeared to influence the work reported in this paper.

Data availability

Data will be made available on request.

Acknowledgements

This study was funded by the Australian Research Council Future Fellowship FT190100801, “Innovative Data Driven Techniques for Structural Condition Monitoring”. The first author acknowledges the financial support from the China Scholarship Council Postgraduate Scholarship Grant 201806120049 and the postgraduate top-up scholarship at Curtin University.

References

[1] Azimi M, Eslamlou AD, Pekcan G. Data-driven structural health monitoring and damage detection through deep learning: State-of-the-art review. Sensors 2020;20:2778.
[2] Oskoui EA, Taylor T, Ansari F. Reference-free dynamic distributed monitoring of damage IN multispan bridges. J Struct Eng 2021;147:04020292.
[3] Peng Z, Li J, Hao H, Nie Z. Improving identifiability of structural damage using higher order responses and phase space technique. Struct Control Health Monit 2021:e2808.
[4] Li J, Hao H, Xia Y, Zhu H-P. Damage assessment of shear connectors with vibration measurements and power spectral density transmissibility. Struct Eng Mech 2015;54:257–89.
[5] Li J, Hao H. A review of recent research advances on structural health monitoring in Western Australia. Structural Monitoring and Maintenance 2016;3:33.
[6] Hu X, Wang B, Ji H. A wireless sensor network-based structural health monitoring system for highway bridges. Comput Aided Civ Inf Eng 2013;28:193–209.
[7] Li H, Ou J, Zhao X, Zhou W, Li H, Zhou Z, et al. Structural health monitoring system for the Shandong Binzhou Yellow River highway bridge. Comput Aided Civ Inf Eng 2006;21:306–17.
[8] Hao H, Bi K, Chen W, Pham TM, Li J. Towards next generation design of sustainable, durable, multi-hazard resistant, resilient, and smart civil engineering structures. Eng Struct 2023;277:115477.
[9] Tan D, Li J, Hao H, Nie Z. Target-free vision-based approach for modal identification of a simply-supported bridge. Eng Struct 2023;279:115586.
[10] Matarazzo TJ, Pakzad SN. Scalable structural modal identification using dynamic sensor network data with STRIDEX. Comput Aided Civ Inf Eng 2018;33:4–20.
[11] Xi R, He Q, Meng X. Bridge monitoring using multi-GNSS observations with high cutoff elevations: A case study. Measurement 2021;168:108303.
[12] Mei Q, Gül M, Shirzad-Ghaleroudkhani N. Towards smart cities: crowdsensing-based monitoring of transportation infrastructure using in-traffic vehicles, Journal of Civil. Struct Health Monit 2020;10:653–65.
[13] Yang Y-B, Lin C, Yau J. Extracting bridge frequencies from the dynamic response of a passing vehicle. J Sound Vib 2004;272:471–93.
[14] Yang Y, Chang K. Extracting the bridge frequencies indirectly from a passing vehicle: Parametric study. Eng Struct 2009;31:2448–59.
[15] Zhan J, Wang Z, Kong X, Xia H, Wang C, Xiang H. A drive-by frequency identification method for simply supported railway bridges using dynamic responses of passing two-axle vehicles. J Bridg Eng 2021;26:04021078.
[16] Singh P, Sadhu A. A hybrid time-frequency method for robust drive-by modal identification of bridges. Eng Struct 2022;266:114624.
[17] Nagayama T, Reksowardojo A, Su D, Mizutani T. Bridge natural frequency estimation by extracting the common vibration component from the responses of two vehicles. Eng Struct 2017;150:821–9.
[18] Yang Y, Wang Z-L, Shi K, Xu H, Wu Y. State-of-the-art of vehicle-based methods for detecting various properties of highway bridges and railway tracks. Int J Struct Stab Dyn 2020;20:2041004.
[19] Eshkevari SS, Matarazzo TJ, Pakzad SN. Bridge modal identification using acceleration measurements within moving vehicles. Mech Syst Sig Process 2020;141:106733.
[20] T.J. Matarazzo, P. Santi, S.N. Pakzad, K. Carter, C. Ratti, B. Moaveni, C. Osgood, N. Jacob, Crowdsensing framework for monitoring bridge vibrations using moving smartphones, Proceedings of the IEEE, 106 (2018) 577-593.

[21] Yang Y, Zhang B, Qian Y, Wu Y. Contact-point response for modal identification of bridges by a moving test vehicle. Int J Struct Stab Dyn 2018;18:1850073.
[22] Peng Z, Li J, Hao H, Xin Y. High-resolution time-frequency representation for instantaneous frequency identification by adaptive Duffing oscillator. Struct Control Health Monit 2020;27:e2635.
[23] Liu J, Chen S, Bergés M, Bielak J, Garrett JH, Kovačević J, et al. Diagnosis algorithms for indirect structural health monitoring of a bridge model via dimensionality reduction. Mech Syst Sig Process 2020;136:106454.
[24] Gkoumas K, Gkoktsi K, Bono F, Galassi MC, Tirelli D. The Way Forward for Indirect Structural Health Monitoring (iSHM) Using Connected and Automated Vehicles in Europe. Infrastructures 2021;6:43.
[25] Malekjafarian A, McGetrick PJ, OBrien EJ. A review of indirect bridge monitoring using passing vehicles. Shock Vib 2015.
[26] Zhan Y, Au FT, Zhang J. Bridge identification and damage detection using contact point response difference of moving vehicle. Struct Control Health Monit 2021: e2837.
[27] Yang Y, Li Y, Chang KC. Constructing the mode shapes of a bridge from a passing vehicle: a theoretical study. Smart Struct Syst 2014;13:797–819.
[28] Malekjafarian A, OBrien EJ. Identification of bridge mode shapes using short time frequency domain decomposition of the responses measured in a passing vehicle. Eng Struct 2014;81:386–97.
[29] Li J, Zhu X, Law S-S, Samali B. Indirect bridge modal parameters identification with one stationary and one moving sensors and stochastic subspace identification. J Sound Vib 2019;446:1–21.
[30] Mei Q, Shirzad-Ghaleroudkhani N, Gül M, Ghahari SF, Taciroglu E. Bridge mode shape identification using moving vehicles at traffic speeds through non-parametric sparse matrix completion. Struct Control Health Monit 2021;28:e2747.
[31] Sadeghi Eshkevari S, Pakzad SN, Takáč M, Matarazzo TJ. Modal identification of bridges using mobile sensors with sparse vibration data. J Eng Mech 2020;146: 04020011.
[32] Wang H, Nagayama T, Nakasuka J, Zhao B, Su D. Extraction of bridge fundamental frequency from estimated vehicle excitation through a particle filter approach. J Sound Vib 2018;428:44–58.
[33] Yang Y, Li Y, Chang K. Using two connected vehicles to measure the frequencies of bridges with rough surface: a theoretical study. Acta Mech 2012;223:1851–61.
[34] Keenahan J, OBrien EJ, McGetrick PJ, Gonzalez A. The use of a dynamic truck–trailer drive-by system to monitor bridge damping. Struct Health Monit 2014;13:143–57.
[35] Huang J, Rao Y, Qiu H, Lei Y. Generalized algorithms for the identification of seismic ground excitations to building structures based on generalized Kalman filtering under unknown input. Adv Struct Eng 2020;23:2163–73.
[36] Lee HJ, Shim JK. Multi-objective optimization of a dual mass flywheel with centrifugal pendulum vibration absorbers in a single-shaft parallel hybrid electric vehicle powertrain for torsional vibration reduction. Mech Syst Sig Process 2022; 163:108152.
[37] Pereyra V, Saunders M, Castillo J. Equispaced Pareto front construction for constrained bi-objective optimization. Math Comput Model 2013;57:2122–31.
[38] Peng Z, Li J, Hao H, Li C. Nonlinear structural damage detection using output-only Volterra series model. Struct Control Health Monit 2021:e2802.
[39] Cahill P, Jaksic V, Keane J, O'Sullivan A, Mathewson A, Ali SF, et al. Effect of road surface, vehicle, and device characteristics on energy harvesting from bridge–vehicle interactions. Comput Aided Civ Inf Eng 2016;31:921–35.